

Journal of Geophysical Research: Atmospheres

RESEARCH ARTICLE

10.1002/2017JD028213

Key Points:

- Study provides tools to evaluate model rain and snow frequency at a range of intensities using CloudSat (94-GHz) radar reflectivities
- Applying tools shows that the Community Earth System Model has excessive near-surface rain and snow frequency, especially for light rain
- Projected precipitation frequency changes in a warmer world are detectable but contain imprints of present-day model biases

Supporting Information:

- Supporting Information S1

Correspondence to:

J. E. Kay,
jennifer.e.kay@colorado.edu

Citation:

Kay, J. E., L'Ecuyer, T., Pendergrass, A., Chepfer, H., Guzman, R., & Yettella, V. (2018). Scale-aware and definition-aware evaluation of modeled near-surface precipitation frequency using CloudSat observations. *Journal of Geophysical Research: Atmospheres*, 123, 4294–4309. <https://doi.org/10.1002/2017JD028213>

Received 16 DEC 2017

Accepted 22 MAR 2018

Accepted article online 30 MAR 2018

Published online 30 APR 2018

Scale-Aware and Definition-Aware Evaluation of Modeled Near-Surface Precipitation Frequency Using CloudSat Observations

Jennifer E. Kay^{1,2} , Tristan L'Ecuyer³ , Angeline Pendergrass⁴ , Helene Chepfer⁵ , Rodrigo Guzman⁵ , and Vineel Yettella^{1,2} 

¹Department of Atmospheric and Oceanic Sciences, University of Colorado Boulder, Boulder, CO, USA, ²Cooperative Institute for Research in Environmental Sciences, University of Colorado Boulder, Boulder, CO, USA, ³Department of Atmospheric and Oceanic Sciences, University of Wisconsin–Madison, Madison, WI, USA, ⁴National Center for Atmospheric Research, Boulder, Colorado, USA, ⁵University Pierre et Marie Curie, Laboratoire de Météorologie Dynamique, Institut Pierre Simon Laplace Ecole Polytechnique, Palaiseau, France

Abstract CloudSat's 94-GHz Cloud Profiling Radar provides unique near-global observations of precipitation frequency and intensity. Here CloudSat-based diagnostics for near-surface precipitation frequency are implemented in publicly available software that is widely used for climate model evaluation. The new diagnostics are “definition aware” and “scale aware.” As a result, the diagnostics enable robust assessment of modeled near-surface precipitation frequency at a range of intensity classes. The new diagnostics are used to evaluate precipitation frequency in a state-of-the-art climate model, the Community Earth System Model version 1 (CESM1). CESM1 rains and snows too frequently, a bias that is especially pronounced for light rain. Conversely, while rare in both observations and CESM1, the heaviest rainfall events occur too infrequently in CESM1. Though the spatial distribution of snowfall events matches observations well, CESM1 also exhibits excessive snow frequency biases. Despite these biases, projected CESM1 changes in reflectivity-based diagnostics provide interesting insights into what a future 94-GHz radar could detect in a warmer world. With 3 °C of global warming, a future CloudSat-class mission would detect substantial conversion of snow to rain at midlatitudes, a narrowing of the Tropical Pacific rain belt, increased light rain in subtropics, and increased snow frequency in polar regions. The future CESM1 simulations also provide evidence that present-day spatial and magnitude biases imprint themselves on precipitation frequency changes. In summary, new precipitation frequency diagnostics for a range of precipitation intensities robustly expose climate model biases and inform expectations for observable future precipitation changes in a warming world.

1. Introduction and Study Goals

Greenhouse gas concentrations are increasing, producing warming and changing the frequency, intensity, and distribution of precipitation. Given the importance of precipitation to climate and water resources, understanding and constraining precipitation changes in a warming world is essential. As summarized in Boucher et al. (2013), the physics controlling precipitation changes in a warming world depend on both dynamics and thermodynamics. Assuming unchanged circulation (fixed dynamics), a warmer atmosphere has an intensified hydrological cycle (Held & Soden, 2006). The resulting “wet-get-wetter, dry-get-drier” phenomena is especially evident in model projections over the tropical ocean (e.g., Held & Soden, 2006) and in midlatitude cyclone composites (e.g., Yettella & Kay, 2017). While useful, the “wet-get-wetter, dry-get-drier” paradigm is not exhaustive. For example, it may not apply over land where surface evaporation is limited (Greve et al., 2014). Even more important, the fixed-dynamics assumption is not valid. The first-order atmospheric circulation response to greenhouse warming is a weakening of the overturning tropical atmospheric circulation that transports heat poleward (e.g., Chou & Neelin, 2004; Vecchi & Soden, 2007). Greenhouse warming also leads to an expansion of the subtropical dry regions (e.g., Lu et al., 2007) and a narrowing of the tropical rain belts (e.g., Byrne & Schneider, 2016).

Global coupled climate models underpin future precipitation projections and serve as test beds for testing theories on precipitation change in a warming world. The primary constraints on precipitation—moisture and energy availability—both depend on temperature, which is reasonably well simulated by climate models

(e.g., Knutti et al., 2013). Yet climate models must parameterize many of the cloud-scale dynamics and processes that produce precipitation. While climate models simulate precipitation amount reasonably well when compared to precipitation radar observations from Tropical Rainfall Measuring Mission (TRMM, Kummerow et al., 2000) and Global Precipitation Climatology Project (GPCP; e.g., Adler et al., 2003; Flato et al., 2013; Pendergrass & Deser, 2017) these same models exhibit large biases in frequency and intensity. Specifically, most models precipitate too frequently with insufficient intensity (e.g., Dai, 2006; Pendergrass & Deser, 2017; Stephens et al., 2010).

Robust observational constraints are required to assess the credibility of precipitation in climate models. Spaceborne precipitation observations have been used for model evaluation on time scales from days to decades (e.g., Hong et al., 2007; Hou et al., 2014; Kim et al., 2009; Kummerow et al., 2000; L'Ecuyer & Stephens, 2007; Nesbitt & Zipser, 2003; Wang et al., 2016; Zhang et al., 2008; Zipser et al., 2006). Over the last decade, CloudSat's Cloud Profiling Radar (CPR) provided the first near-global precipitation observations from spaceborne radar (Behrangi et al., 2012; Berg et al., 2010; Stephens et al., 2008). While strong radar beam attenuation limits the use of CPR reflectivities in heavy precipitation, CloudSat measures precipitation frequency everywhere, including both light and heavy precipitation frequency (Ellis et al., 2009). Previous studies have demonstrated the value of reflectivity-based evaluation of model precipitation using CloudSat (e.g., Bodas-Salcedo et al., 2008; Jing et al., 2017; Marchand et al., 2009; Nam et al., 2014; Stephens et al., 2010; Suzuki et al., 2015; Zhang et al., 2010), though uncertainties exist [e.g., owing to inconsistencies in the drop size distribution assumptions applied in the radar forward model, sensitivity to the definition of subgrid precipitation fraction (Di Michele et al., 2012), and in upscaling the CloudSat observations to coarser model resolutions (Stephens et al., 2010)].

Recognizing previous work, we argue that CloudSat has unrealized potential for evaluation of model precipitation. Why? What have previous studies missed? What are the criteria for robust and easily interpretable diagnostics to evaluate climate model precipitation? First, diagnostics must be "definition aware." In other words, the definition of precipitation must be the same. Spaceborne radars have differing capacities to measure light and heavy precipitation. For example, 14-GHz precipitation radars like that on TRMM do not detect light precipitation while 94-GHz cloud radars like CloudSat saturate in heavy precipitation (e.g., Figure 3, Berg et al., 2010). Neglecting radar sensitivity when evaluating models will result in erroneous conclusions about model performance. Second, diagnostics must be "scale aware." In other words, the spatiotemporal scale on which precipitation is assessed should be the same. Finally, diagnostics need to be easy to interpret. For example, it is extremely beneficial to have diagnostics that are mappable and enable comparison of precipitation spatial distributions. No previous study evaluating climate model precipitation has addressed these three criteria simultaneously.

Motivated to provide robust and mappable precipitation diagnostics for the climate modeling community, this study has two goals. First, we introduce mappable scale-aware and definition-aware metrics for near-surface precipitation frequency for a range of precipitation intensities based on the CloudSat 2C-PRECIP (2CPC) product (Haynes et al., 2009). We then use these diagnostics and corresponding observations to evaluate present-day climate model simulations. This first goal addresses the current lack of robust and easily mappable precipitation diagnostics for climate models. Comparing precipitation frequency defined using radar reflectivity thresholds enables a direct comparison between the raw CloudSat observations and model precipitation, while minimizing retrieval assumptions. The approach is more robust than using CloudSat-retrieved precipitation amounts, which require many retrieval assumptions (e.g., specification of drop size distributions that may not be consistent with those adopted by the model). Since atmospheric radiative cooling constrains global precipitation, the diagnostics for total and heavy precipitation frequency introduced here provide useful constraints to dissect model biases (Stephens & Ellis, 2008; Stephens et al., 2010). In addition, the partitioning between liquid and frozen precipitation provides new diagnostics of direct relevance to planetary albedo (e.g., Dery & Brown, 2007; Flanner et al., 2011), water storage in seasonal snow (e.g., Barnett, Adam, & Lettenmaier, 2005), and ice sheet mass balance (e.g., Palmer et al., 2014; Rignot et al., 2011).

Building on the first present-day model evaluation goal, our second goal is to use our new diagnostics to assess near-surface precipitation frequency changes that would be observable by a radar mission equivalent to CloudSat but launched in a warmer world. While precipitation observations can constrain present-

day precipitation distributions, observational records are often too short to discern meaningful trends and cannot be used to predict future changes. As such, model simulations provide unique and interesting insights into what we might have observed in the past and what we might observe in the warmer world. This second goal also builds on the first goal by assessing a key reliability question: Do current climate precipitation biases imprint themselves on future precipitation projections (e.g., as suggested by Bony et al., 2013)?

2. Methods

2.1. New Near-Surface Precipitation Frequency Diagnostics for Model Evaluation

In this study, we develop new CloudSat-based precipitation diagnostics within the framework of the community simulator package Cloud Feedbacks Model Intercomparison Project (CFMIP) Observational Simulator Package (COSP, Bodas-Salcedo et al., 2011). COSP is a model agnostic software package that has been run in a range of models: from climate models to cloud resolving models. To understand the value of the simulators in COSP for model applications, it is first important to recognize that while they may have the same name, geophysical parameters in models and observations do not have the same meaning. There are fundamental differences between the modeled and retrieved quantities including: finite observational detection thresholds, differences between instrument fields of view and model resolution, sampling differences, and even the physical representation of the relevant processes. As a result, with the exception of the most basic integrated quantities, use of satellite simulators, like those available in COSP, enables “definition-aware” and “scale-aware” comparison between model outputs and satellite observations.

COSP has been used extensively for evaluation of clouds in climate models (e.g., Webb et al., 2017). In contrast, COSP precipitation diagnostics have been less widely used by the modeling community. One reason might be because the only precipitation-relevant diagnostics available in COSP are CloudSat Cumulative Frequency by Altitude Diagrams (CFADs). CFADs composite vertical profiles of radar reflectivity to provide a statistical overview of the vertical structure of hydrometeors (i.e., clouds and precipitation) in a domain (Yuter & Houze, 1995). While a staple for radar reflectivity experts, CFADs are not intuitive to many scientists in the climate modeling community. In addition, CFADs are not easily mapped.

In this study, we introduce new precipitation diagnostics within COSP that enable assessment of near-surface precipitation frequency. The new diagnostics are parallel to the thresholds and methodology adopted in a standard CloudSat product 2CPC. Described in Haynes et al. (2009), the 2CPC precipitation diagnostics quantify the occurrence frequency of liquid and solid precipitation in a range of intensity classes. The new diagnostics are based on radar reflectivities from the radar simulator in COSP: Quickbeam (Haynes et al., 2007). Quickbeam is a plane-parallel radar forward model that simulates W-band (94 GHz) reflectivities equivalent to those observed by CloudSat. Attenuation-corrected reflectivities for each range bin of a downward looking radar with specified resolution are computed via the standard radar equation. Scattering and attenuation from an adjustable number of different cloud and precipitating hydrometer species with appropriate density and size distribution assumptions can be modeled by linking to precomputed look-up tables. A correction is made to account for multiple scattering effects using off-line calculations from Hogan and Battaglia (2008).

The methodology we introduce here for comparing precipitation frequency in models and observations is both definition aware and scale aware. Our methods are “definition aware” because we use the same 2CPC-based definitions of precipitation for the model and the observations. We apply the Haynes et al. (2009) 2CPC thresholds over ocean and thresholds from Smalley et al. (2014) over land. While precipitation intensity depends on the radar reflectivity, precipitation phase is classified using the melted precipitation fraction over the ocean and the surface air temperature over the land. Over the ocean, 2CPC invokes a melting-layer model following Fabry and Zawadzki (1995) to partition liquid and ice below the freezing level. Rain is identified when the near-surface melted fraction is at least 0.9. Snow is identified when the near-surface melted fraction is less than 0.1. The fraction-based precipitation phase classification strategy of 2CPC is also applied within the model. Our methods are also “scale aware” because we use the subcolumn generator to enable comparison of model and observations at the individual profile scale. In other words, we “downscale” the model grid box mean values to the observations, as

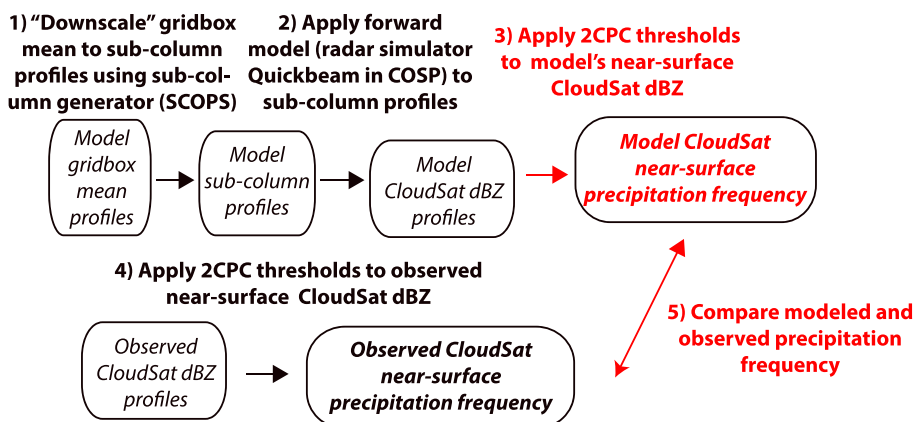


Figure 1. Schematic showing methods used in this study to make “scale-aware” and “definition-aware” comparisons between observed and modeled CloudSat near-surface precipitation frequency. Text in red indicate new additions to the existing COSP precipitation infrastructure and new comparisons developed by this study.

opposed to upscaling the CloudSat observations to coarser model resolutions as has been done in previous studies (Stephens et al., 2010). Our “downscaling strategy” compares model subcolumns to observations taken on the satellite footprint. The imperfect assumption we make is that the subcolumns represent the same spatial scale as the satellite observations. Given the large difference in spatial scales represented by global climate models and satellite observations, making comparisons on the same spatial scale is challenging. The methods we use and assumptions that we make to be “scale aware” are shared with many satellite simulator studies (e.g., Bodas-Salcedo et al., 2011).

A step-by-step illustration of our methods is provided in Figure 1. We begin with the grid box mean profiles from a model. We then use the subcolumn generator embedded within COSP (Klein & Jakob, 1999) to produce a large number of subgrid-scale cloud and precipitation profiles (“subcolumns”) within each model grid box (step 1). These COSP-generated subcolumns are consistent with the model’s grid box mean ice and liquid water contents, drop sizes, precipitation amount, cloud fraction, and overlap assumptions. We note that the COSP-generated subcolumns are only used to calculate COSP diagnostics. Next, we input the subcolumn profiles into the radar forward model to produce radar reflectivity profiles (step 2). Next, we apply ocean-specific (Haynes et al., 2009) and land-specific (Smalley et al., 2014) thresholds from 2CPC to the individual radar reflectivity profiles. Specifically, we assign each subcolumn profile a precipitation flag based on the near-surface (i.e., 480–960 m above ground level over the ocean; 960–1,440 m over the land) radar reflectivity. The same thresholds are applied to the model (step 3) as are applied to the observations (step 4). Finally, we calculate the precipitation occurrence frequency. For each precipitation flag, we divide the number of profiles with that precipitation flag by the total number of profiles considered.

2.2. Model Simulations With CloudSat Near-Surface Precipitation Frequency Diagnostics

We implemented the new precipitation frequency diagnostics within the Community Earth System Model (CESM) version 1 with the Community Atmosphere Model version 5 (CESM1; Hurrell et al., 2013) and COSP version 1.4. COSP version 1.4 is available in CESM1 (Kay et al., 2016), including CESM-specific modifications for radiatively active snow (English et al., 2014; Kay et al., 2012). While this study uses COSP1.4, the CloudSat-based diagnostics described in this paper will be released to the broader scientific community within the latest COSP version: COSP 2 (Swales et al., 2018).

Of particular relevance to this study is the representation of precipitation processes in CESM1. Precipitation in CESM1 is diagnostic, is not advected, has a Marshall-Palmer size distribution, and has no subgrid-scale variability (Morrison & Gettelman, 2008). Snow and rain are diagnosed separately and can both occur in a grid cell. A description of the integration of cloud and precipitation processes in CAM5 can be found in Park et al. (2014).

We ran simulations to assess both present-day and late 21st century distributions of near-surface precipitation frequency in CESM1 (Table 1). All simulations use 250 subcolumns for each model grid box, a value

Table 1*Climate Model Simulations Used in This Study*

Simulation name	Details
CESM1 present day	Fully coupled simulation, 2011–2025
CESM1 future	Fully coupled simulation, 2081–2095, ~3 °C global warming when compared to CESM1 present day
CAM5 present day	Atmosphere-only simulation, 2006–2015

Note. All simulations use the Community Earth System Model version 1 (CESM1) with the Community Atmosphere Model version 5 (CAM5; Hurrell et al., 2013). All simulations were initialized using restarts from CESM1-CAM5 Large Ensemble (Kay et al., 2015) member 1. All precipitation diagnostics were calculated hourly using 250 subcolumns.

that is excessive for the annual multiyear comparisons made in this study. CESM1 diagnostics for precipitation frequency are produced for every radiation time step (i.e., every hour).

We evaluate CESM1 present-day simulations using comparable CloudSat observations. Specifically, we use gridded observations of 2CPC CloudSat near-surface precipitation frequency (Ellis et al., 2009) for 11 years from June 2006 to May 2016. These gridded observations will be placed on CFMIP-OBS (on CLIMSERV) and obs4MIPS (Teixeira et al., 2014) in netcdf format. In April 2011, CloudSat experienced a battery failure. As a result, there are no CloudSat observations available for May through October in 2011. In late October 2011, CloudSat resumed operations in Daylight-only Operations (Do-Op) mode. As a result, only daytime CloudSat CPR data are available starting in November 2011. For the annual multiyear climatological comparisons presented in this study, the differences introduced by using CloudSat data from the first four full years of the mission (June 2006 to May 2010) or a longer period including data collected in Do-Op mode (June 2006 to May 2016) are order 0.1% for global annual means of precipitation frequency. As we will show, these differences are small when compared to CESM1 biases.

We focused on evaluation of near-surface rain and snow frequency at a range of intensities (Table 2). The precipitation types were simplified from the original precipitation classes in 2CPC. The lightest rain class examined was for CloudSat light rain, which is drizzle. Over the ocean, the reflectivity threshold for drizzle (near-surface reflectivity less than 0 dBZ) is consistent with rain rates of less than ~0.72 mm/day (Haynes et al. 2009). Over the ocean only, CloudSat also provides a very robust, albeit binary, measure of heavy rain, that is, the complete attenuation of the radar beam. Indeed, the combination of multiple scattering and full attenuation enables unequivocal identification of when heavy rainfall is present (Battaglia et al., 2008). The rainfall amounts associated with CloudSat heavy rain are hard to define and vary with freezing level, but occur at rainfall rates as small as ~72 mm/day in the Tropics and as large as ~240 mm/day at higher latitudes. To help translate CloudSat radar reflectivities into precipitation units that are more familiar to many readers, we provide probability distribution functions of simulated CloudSat radar reflectivity and precipitation amount in CESM1 (Figure 2). In addition to providing sample conversion from radar reflectivity to precipitation amount, the distributions shown in Figure 2 also demonstrate that the CloudSat reflectivity-based precipitation frequency diagnostics applied in this study are sensitive to all daily mean precipitation accumulation values simulated in CESM1.

Table 2*CloudSat-Based Precipitation Classes Used in This Study*

Name	Thresholds
CloudSat light rain	$-15 \text{ dBZ} < \text{dBZ} < 0 \text{ dBZ}$ and $F_{\text{ice}} < 0.1$ over ocean; $-15 \text{ dBZ} < \text{dBZ} < 5 \text{ dBZ}$ and $T_{\text{air-surf}} > 275$ over land
CloudSat rain	$> 0 \text{ dBZ}$ and $F_{\text{ice}} < 0.1$ over ocean; $> 5 \text{ dBZ}$ or heavy attenuated indicated by maximum dBZ in the profile $> 10 \text{ dBZ}$ or two-way radar beam attenuation $> 30 \text{ dBZ}$ and $T_{\text{air-surf}} > 275$ over land
CloudSat heavy rain	Two-way radar beam attenuation $> 40 \text{ dBZ}$ and $F_{\text{ice}} < 0.1$ over ocean
CloudSat light snow	$-15 \text{ dBZ} < \text{dBZ} < -5 \text{ dBZ}$ and $F_{\text{ice}} > 0.9$ over ocean; $-15 \text{ dBZ} < \text{dBZ} < -5 \text{ dBZ}$ and $T_{\text{air-surf}} < 273 \text{ K}$ over land
CloudSat snow	$> -5 \text{ dBZ}$ and $F_{\text{ice}} > 0.9$ over ocean; $> -5 \text{ dBZ}$ and $T_{\text{air-surf}} < 273$ over land

Note. Over the ocean, precipitation classes are defined by applying thresholds to the near-surface (480–960 m) unattenuated radar reflectivity (dBZ) and the fraction of ice (F_{ice}), following the 2CPC algorithm (Haynes et al., 2009). The same thresholds are applied in both model simulations and in observations. Over the land, precipitation classes are defined by applying thresholds to the near-surface (960–1,440 m) attenuated radar reflectivity (dBZ) and the surface air temperature ($T_{\text{air-surf}}$) following Smalley et al. (2014).

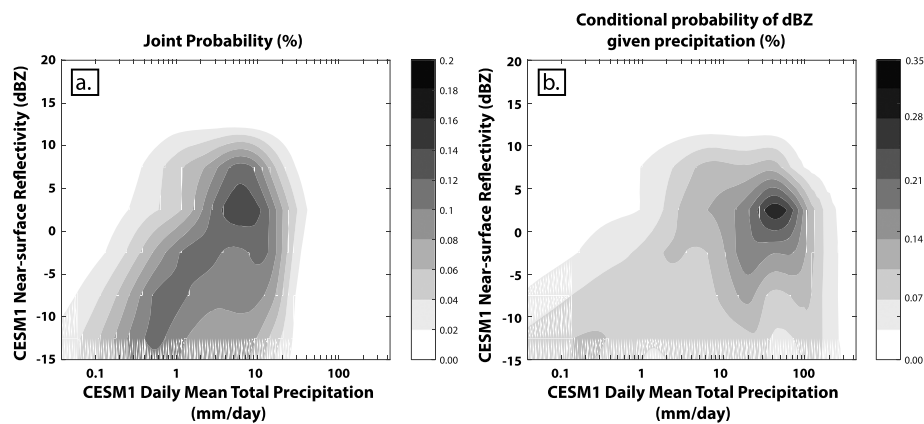


Figure 2. CESM1 probability distribution functions of daily mean simulated near-surface (480–960 m) CloudSat radar reflectivity (dBZ) and daily mean total precipitation: (a) joint probability, (b) conditional probability of dBZ given daily mean total precipitation. Data are from the CESM1 present-day simulation (Table 1).

2.3. Sources of Uncertainty for the Diagnostics Used in This Study

By construct, the precipitation frequency diagnostics introduced in this study are directly comparable to CloudSat observations. Nevertheless, instrument noise and diurnal sampling can both introduce uncertainty. To help quantify the influence of these two sources of uncertainty and assess if they are first-order drivers of detected differences, we completed sensitivity tests using CESM1 (see supporting information). The CESM1 sensitivity tests revealed that instrument noise and diurnal sampling contribute little to the model biases identified in this work. Based on these CESM1 sensitivity tests and previous work, differences between modeled and observed precipitation frequency identified in this study originate from three sources: (1) biases in model precipitation frequency, (2) biases in model microphysics that affect the forward calculation of radar

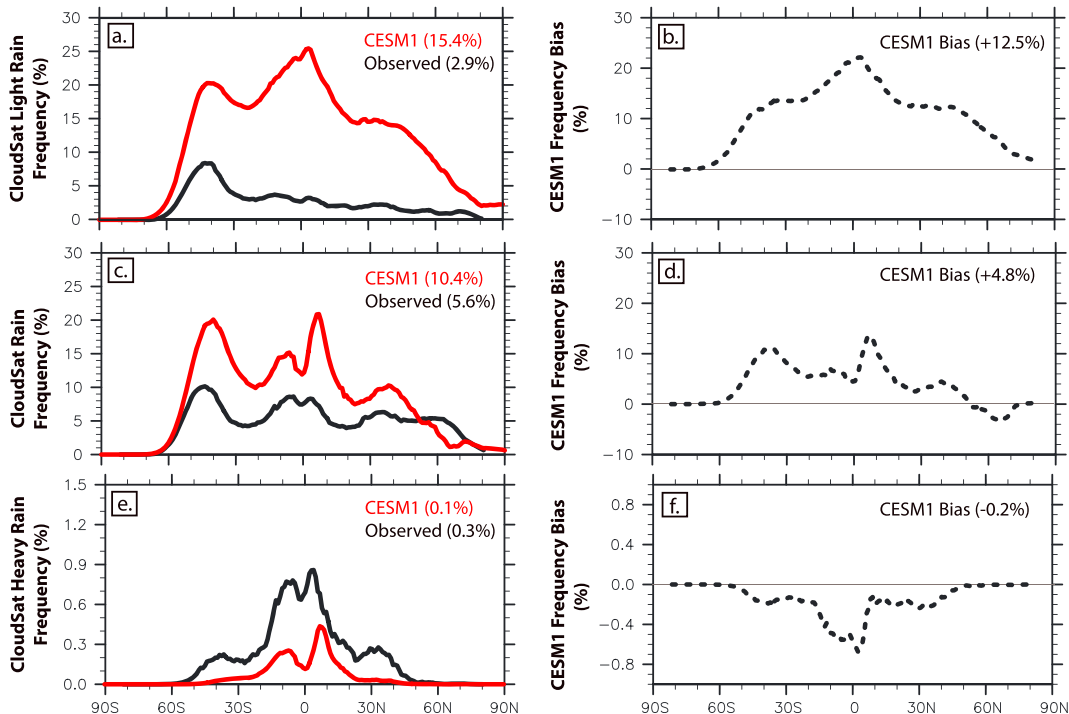


Figure 3. Present annual zonal mean near-surface rain: (a) CESM1 and observed CloudSat light rain frequency, (b) CESM1 light rain frequency bias, (c) CESM1 and observed CloudSat rain frequency, (d) CESM1 CloudSat rain frequency bias, (e) CESM1 and observed CloudSat heavy rain, (f) CESM1 CloudSat heavy rain bias. CESM1 values are from simulation named "CESM1 Present" (see Table 1 for details). Reflectivity-based definitions of the three reported rain classes are the same in observations and CESM1 (see Table 2). CloudSat observations are from 2006 to 2015. Global annual mean values are reported in parenthesis.

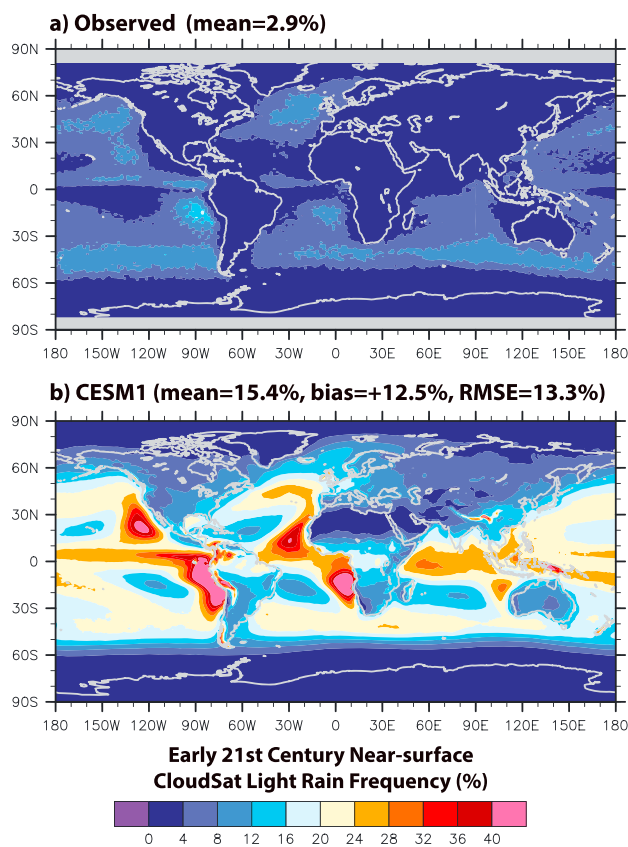


Figure 4. Global map of present-day CloudSat light rain frequency: (a) observed, (b) CESM1. CESM1 values are from simulation named “CESM1 Present” (see Table 1 for details). CloudSat light rain is defined as the near-surface (720–960 m) having a radar reflectivity as follows: $-15 < \text{dBZ} < 0$ (Table 2).

rain frequency are largest for the lightest rain intensity class examined—CloudSat light rain. CESM1 produces CloudSat light rain ~ 5 times more often than observed in the global annual mean (Figure 3a). Zonal annual mean plots show CloudSat light rain occurs too frequently at all latitudes in CESM1 (Figure 3a). In addition to magnitude biases, the maximum CloudSat light rain frequency occurs at the wrong latitude. While the observed CloudSat light rain peaks in Southern Hemisphere midlatitude storm track, CESM1 produces the maximum CloudSat light rain in the Tropics close to the equator (Figure 3a). Global maps show that the overestimation of CloudSat light rain occurrence is especially prominent in the subtropical low cloud decks off the West coasts of the Americas and Africa, the intertropical convergence zone (ITCZ), and equatorial land areas with convection (Figure 4).

Similar to CESM1 CloudSat light rain biases, CloudSat rain also occurs too often in CESM1. Specifically, it rains ~ 2 times more frequently in CESM1 than it does in CloudSat observations in the global annual mean. While the global annual mean primarily reflects excessive rain over the ocean and tropical land, insufficient CloudSat rain falls over midlatitude land (e.g., 50–70°N in Figure 3c). Insufficient CloudSat rain over midlatitude land regions in CESM1 is a consequence of the relatively high 5-dBZ threshold required to detect CloudSat rain over land (Table 2). While CESM1 rains too often, the CESM1-modeled zonal mean pattern of CloudSat rain frequency has many similarities with the observations. Both the model and observations exhibit maxima in zonal mean CloudSat rain frequency in the tropical rain belts and the midlatitude storm tracks (Figures 3c and 5). Both CESM1 and observations show greater rain frequency in the Southern midlatitude storm track than in the Northern midlatitude storm track. While CloudSat rain occurs more frequently north of the equator than south of the equator in both observations and CESM1, CESM1 has excessive CloudSat rain frequency at 5°S, consistent with the well-known “double ITCZ” bias.

reflectivity, and (3) uncertainty in the generation of subcolumns. The CESM1 biases shown here are an aggregate of these three effects, and distinguishing between them requires methods that are beyond the scope of this study.

3. Results

3.1. Evaluation of CESM1 Present-Day Precipitation Frequency Using CloudSat Observations

3.1.1. Modeled and Observed Rain Frequency

We begin by evaluating rain frequency in present-day fully coupled CESM1 simulations (Table 1). Specifically, we compare CloudSat-observed and CloudSat-simulated near-surface rain frequency. Our evaluation of rain frequency includes three reflectivity-based rain intensity classes: CloudSat light rain, CloudSat rain, and CloudSat heavy rain (Table 2). Global mean comparisons indicate that CESM1 has excessive CloudSat light rain (Figures 3a and 3b, frequency bias +12.5%) and CloudSat rain (Figures 3c and 3d, frequency bias +4.8%), but insufficient CloudSat heavy rain (Figures 3e and 3f, frequency bias -0.2%). Excessive CloudSat light rain is an especially pronounced CESM1 bias. For example, in the annual global mean CESM1 produces CloudSat light rain (15.4%) more frequently than CloudSat rain (10.4%). In contrast, annual global mean CloudSat observations show that CloudSat rain (5.6%) occurs more frequently than CloudSat light rain (2.9%). While excessive CloudSat light rain frequency biases are particularly striking, rain frequency biases occur in all three rain intensity classes. We next discuss each rain intensity class in turn, including evaluation of zonal mean distributions (Figure 3) and global spatial distributions for CloudSat light rain frequency (Figure 4), CloudSat rain frequency (Figure 5), and CloudSat heavy rain frequency (Figure 6).

As introduced above, differences between observed and modeled rain frequency are largest for the lightest rain intensity class examined—CloudSat light rain. CESM1 produces CloudSat light rain ~ 5 times more often than observed in the global annual mean (Figure 3a). Zonal annual mean plots show CloudSat light rain occurs too frequently at all latitudes in CESM1 (Figure 3a). In addition to magnitude biases, the maximum CloudSat light rain frequency occurs at the wrong latitude. While the observed CloudSat light rain peaks in Southern Hemisphere midlatitude storm track, CESM1 produces the maximum CloudSat light rain in the Tropics close to the equator (Figure 3a). Global maps show that the overestimation of CloudSat light rain occurrence is especially prominent in the subtropical low cloud decks off the West coasts of the Americas and Africa, the intertropical convergence zone (ITCZ), and equatorial land areas with convection (Figure 4).

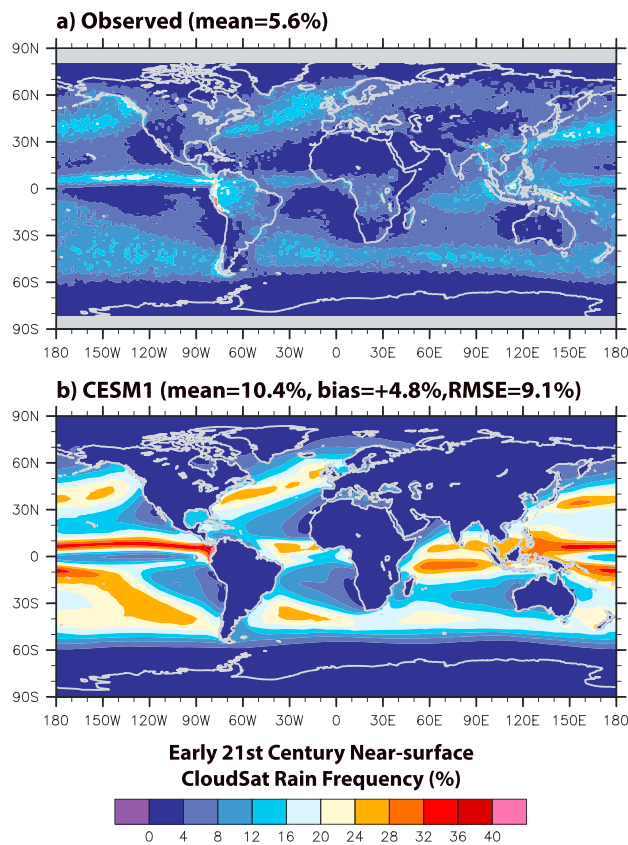


Figure 5. Global map of present-day CloudSat near-surface rain frequency: (a) observed, (b) CESM1. CESM1 values are from simulation named “CESM1 Present” (see Table 1 for details). CloudSat rain is defined as CloudSat reflectivity greater than 0 dBZ (Table 2).

to the fully coupled CESM1 simulation.

3.1.2. Modeled and Observed Snow Frequency

Having evaluated CESM1 rain frequency, we next evaluate CESM1 near-surface snow frequency. We assess snow frequency in two intensity classes—CloudSat light snow and CloudSat snow, once again using radar reflectivity-based thresholds (Table 2). Unsurprisingly, CloudSat snow and CloudSat light snow primarily occur at high latitudes: greater than $\sim 30^\circ\text{N}$ and $\sim 40^\circ\text{S}$ (Figure 7). Both the observations and CESM1 have the largest snow frequencies in the midlatitude storm tracks, especially over the Southern Ocean. Similar to what was found for rain frequency (Figure 3), CESM1 has excessive snow frequency at all latitudes when compared to observations (Figure 7). The absolute frequency and global mean bias are both ~ 2 times larger for CloudSat snow than for CloudSat light snow. Finally, differences in the CloudSat-simulated snow between the fully coupled CESM1 and atmosphere-only CAM5 simulations are negligible (not shown). Thus, as for rain, snow frequency biases in CESM1 are unaffected by coupling with the ocean and appear to originate from the atmospheric model.

Maps of snowfall frequency patterns indicate that even though it snows too frequently in CESM1, the geographic distribution of CESM1 snow events often matches CloudSat observations (Figure 8). An example of a particularly striking spatial pattern match between CESM1 and observations occurs in the Southern Hemisphere storm track where CESM1 reproduces the observed meridional minimum in CloudSat Snow occurrence in the Western South Atlantic ($60\text{--}70^\circ\text{S}$, $30\text{--}60^\circ\text{W}$). Less surprising but still encouraging, CloudSat light snow and CloudSat snow occur at high elevations (e.g., the Himalayas and the Rockies) in both the model and the observations. Finally, at the highest latitudes and altitudes on the planet (i.e., over the Greenland and Antarctic ice sheets), both CESM1 and observations show increasing occurrence of lighter snow (i.e., more CloudSat light snow frequency as compared to CloudSat snow frequency). Then again,

In contrast to excessive CloudSat light rain and CloudSat rain frequency biases, CESM1 has insufficient CloudSat heavy rain frequency. In other words, CloudSat heavy rain is underestimated in CESM1 when compared to observations. This result implies that CESM1 has insufficient rain intensity. In the global annual mean, observed CloudSat heavy rains events are rare (0.3%) when compared to observed CloudSat rain events (5.6%) and observed CloudSat light rain events (2.9%). In both observations and CESM1, CloudSat heavy rain is largest in the tropics and decreases with increasing latitude (Figure 3e). Like observations, CloudSat heavy rain is largest in the northern branch of the ITCZ in CESM1. Yet, in this region, CloudSat heavy rain occurs ~ 2 times more frequently in observations than it does in CESM1. CloudSat heavy rain is 3–5 times more frequent in observations than in CESM1 at latitudes as far poleward as 40° in both hemispheres.

Next, we briefly address the influence of ocean coupling on CESM1 rain frequency by comparing fully coupled and atmosphere-only simulations. Because CloudSat rain frequency is minimally affected by ocean coupling, we do not show plots of the results. All biases are qualitatively and for the most part quantitatively similar in the fully coupled and atmosphere-only simulations. Like the fully coupled CESM1 simulation, the atmosphere-only CAM5 simulation exhibits excessive CloudSat rain and CloudSat light rain frequency and insufficient CloudSat heavy rain frequency. Similar biases in fully coupled and atmosphere-only simulations suggest that rain frequency biases largely originate from the atmospheric model. Ocean coupling does have a small influence on rain frequency in the Tropics. When compared with the fully coupled CESM1, the atmosphere-only CAM5 has more CloudSat rain and CloudSat heavy rain in the Northern Hemisphere tropical rain belt and less in the Southern Hemisphere tropical rain belt. In other words, the CloudSat rain frequency bias associated with the double ITCZ bias was slightly improved in the atmosphere-only CAM5 simulation as compared

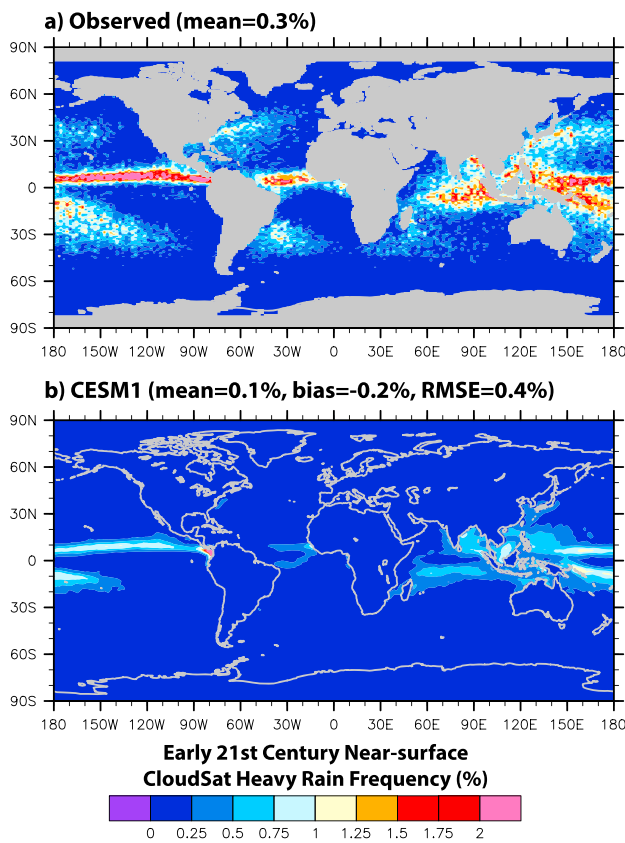


Figure 6. Global map of present-day CloudSat heavy rain frequency: (a) observed, (b) CESM1. CESM1 values from simulation named “CESM1 Present” (see Table 1 for details). CloudSat heavy rain occurs when the path-integrated attenuation (PIA) greater than 40 dBZ. CloudSat heavy rain is only available over oceans in observations.

there are regions where the spatial pattern match is not as good between CESM1 and observations. For example, CESM1 has particularly excessive snow frequency in Northern Europe and Russia downwind of the North Atlantic storm track when compared to observations (Figures 8c and 8d).

3.2. Future Changes in Near-Surface CloudSat Precipitation Frequency

3.2.1. Global-Scale Changes in Precipitation Frequency

Having evaluated present-day CloudSat precipitation frequency in CESM1, we next quantify changes in CloudSat precipitation frequency predicted by CESM1 over the 21st century. Specifically, we compare precipitation frequency in the late 21st century (the average over 2080–2095) with the present (the average over 2010–2025) using fully coupled CESM1 simulations (Table 1). Through this comparison, we are able to address the second goal of our work: quantifying the precipitation frequency changes in CESM1 that would be detected by a CloudSat-class spaceborne radar and assessing the imprint of present-day biases on future change.

We begin with zonal mean plots of precipitation frequency change for a range of intensities (Figure 9). Zonal-mean CESM-projected 21st century changes in CloudSat rain frequency and CloudSat light rain frequency are negligible in the Tropical (Figure 9a). In contrast, zonal-mean CloudSat light rain increases in the subtropics (Figure 9b) and zonal mean Tropical CloudSat heavy rain frequency increases by a factor of ~ 2 (Figure 9c). In the midlatitudes of both hemispheres, CloudSat rain frequency increases (Figures 9a and 9b) and CloudSat snow frequency decreases (Figures 9d and 9e) consistent with poleward shifts of isotherms. Snow frequency decreases at the expense of rain frequency increases are largest over the Southern Ocean. For example, CloudSat snow frequency at 55°S reduces to two thirds its present-day value (30%) by the 2080s. The only latitudes with CloudSat snow frequency increases are

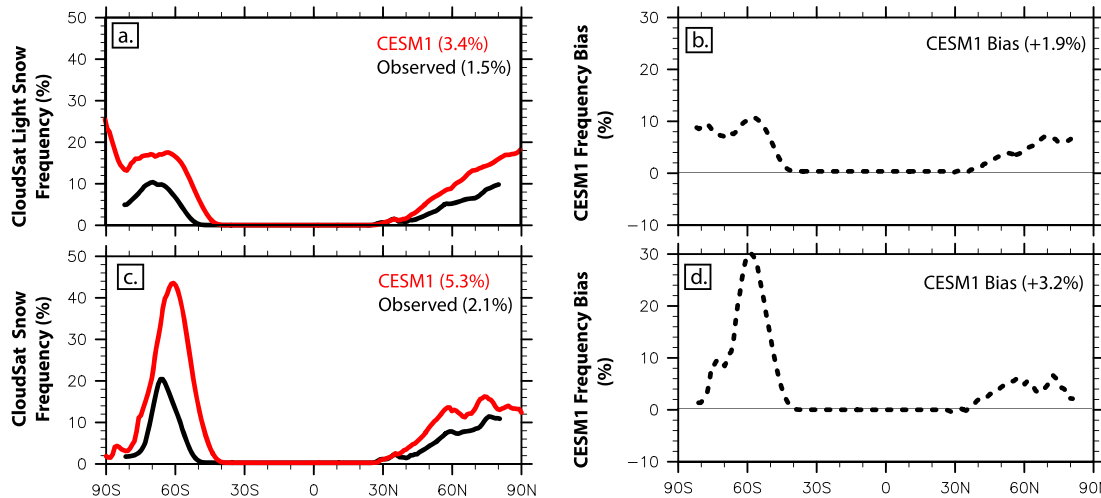


Figure 7. Present-day zonal mean near-surface snow: (a) CESM1 and observed CloudSat light snow frequency, (b) CESM1 light snow frequency bias, (c) CESM1 and observed CloudSat snow frequency, (d) CESM1 CloudSat snow frequency bias. CESM1 values from simulation named “CESM1 Present” (see Table 1 for details). Reflectivity-based definition of CloudSat light snow and snow are the same in observations and CESM1 (see Table 2). Global annual mean values are reported in parenthesis.

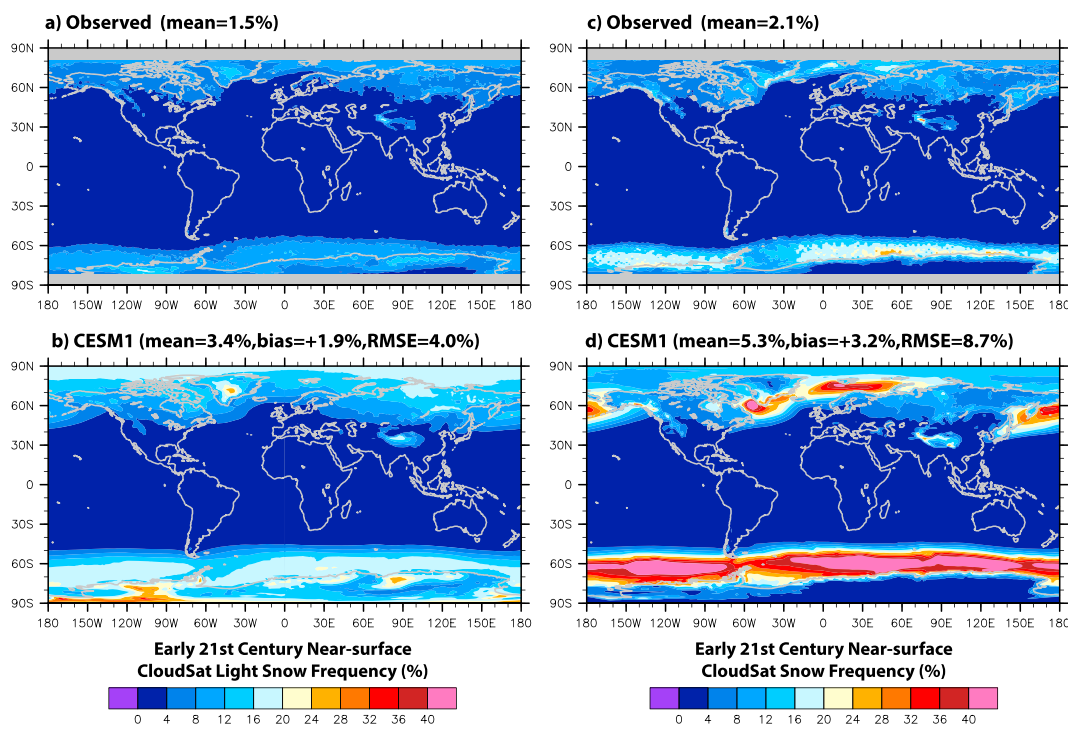


Figure 8. Global map of present-day near-surface snow frequency: (a) observed CloudSat light snow, (b) CESM1 CloudSat light snow, (c) observed CloudSat snow, (d) CESM1 CloudSat snow. CESM1 values from simulation named “CESM1 present” (see Table 1 for details). CloudSat light snow and CloudSat snow definitions are based on reflectivity and fraction of ice present (see Table 2).

the polar latitudes ($>70^\circ$) of both hemispheres, especially in the Arctic (Figure 9d). While zonal means provide a first-order quantification of the 21st century CESM1 precipitation frequency changes, zonal means obscure spatial patterns following land-ocean boundaries, topography, and azonal atmospheric circulations. As such, we next examine global maps of the precipitation frequency change (2080s minus 2010s) for both rain (Figure 10) and snow (Figure 11).

Global maps of the 21st century change in CESM1 rain frequency (Figure 10) show rich spatial structure in the tropics and subtropics not evident in the zonal means. Over the eastern subtropical Pacific and Atlantic Oceans, where low clouds dominate, CloudSat light rain increases over the 21st century (Figure 10a). Over the Amazon, CloudSat light rain frequency decreases (Figure 10b). Over the Tropical Pacific Ocean, off-equatorial CloudSat rain decreases and equatorial CloudSat rain increases. Finally, CloudSat heavy rain changes occur primarily in the Tropics (Figure 10c), with spatial structure similar to present-day patterns of CloudSat heavy rain (Figure 5b).

In the extratropics, precipitation 21st century frequency changes are largest over the midlatitude storm tracks, over high elevations, and at high latitudes (Figures 10 and 11). Midlatitude rain frequency increases and snow frequency decreases evident in the zonal mean (Figure 9) are produced by oceanic storm track regions and nearby land regions (Figure 10). While most midlatitude CloudSat rain changes over land are small, high-elevation mountain ranges (e.g., Rockies, Himalayas) show large reductions in CloudSat snow and large increases in CloudSat light rain over the 21st century. At high latitudes, CloudSat rain and CloudSat snow frequency increases are largest over the Arctic Ocean, near the coast of Antarctica in the Southern Ocean, and over Greenland and Antarctica.

3.2.2. Tropical Pacific Changes in Precipitation Frequency

CESM1 simulations reveal many locations with the 21st century precipitation frequency changes that, if realistic, would be detectable by a future CloudSat-class 94-GHz spaceborne radar mission. A stated goal of this study is to explore the influence that the present-day biases might have on the 21st century projected changes. Relating present-day biases with future changes is best done at a regional scale.

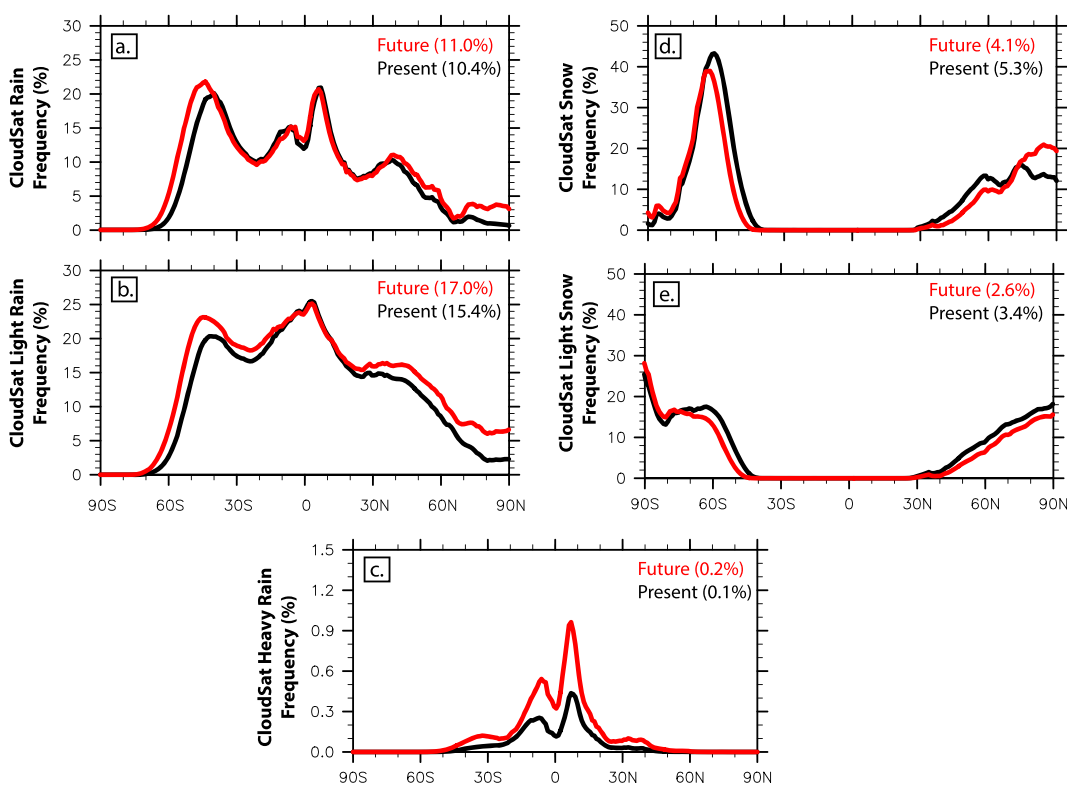


Figure 9. Present-day and future zonal annual mean near-surface precipitation frequency in CESM1: (a) CloudSat rain frequency, (b) CloudSat light rain frequency, (c) CloudSat heavy rain frequency, (d) CloudSat snow frequency, (e) CloudSat light snow frequency. Definitions of precipitation frequency are based on radar reflectivity and ice fraction (see Table 2). Global annual mean values are reported in parenthesis.

To keep our efforts focused, we examine biases and future changes in one region of interest: The tropical and subtropical Pacific Ocean. This region illustrates the power of having rain frequency diagnostics at a range of precipitation intensities. Figure 12 compares regional maps over the Tropical Pacific Ocean for CloudSat light rain, CloudSat rain, and CloudSat heavy rain. By simultaneously plotting present-day observations, present-day CESM1 and CESM1 21st century changes (2080s minus 2010s), we clearly see that the spatial distribution of rain frequency and its change over the 21st century depends strongly on rain intensity.

The largest CloudSat light rain frequencies in the Tropical Pacific Occur off the West Coast of the Americas in shallow convective regimes where low clouds dominate. When compared to observations, CESM1 overestimates CloudSat light rain in these regions by a factor of 5. Additionally, CESM1 light rain occurs too close to the coast when compared to observations. Over the 21st century, CESM1 CloudSat light rain frequency increases and moves away from the coast toward the central Pacific.

Over the Tropical Pacific, the ITCZ controls the spatial distribution of CloudSat rain frequencies in both observations and CESM1. While CESM1 overestimates rain frequency in both the southern and the northern branches of the ITCZ, the spatial distribution of CloudSat rain in CESM1 is worse south of the equator than it is north of the equator. In particular, the Southern branch of the ITCZ is too meridional and also extends too far into the central Pacific. Over the 21st century, off-equatorial CloudSat rain decreases and equatorial CloudSat rain increases. This ITCZ narrowing equatorward is most apparent in the Central and Eastern Tropical Pacific. Because the southern branch of the ITCZ has worse present-day spatial pattern biases, the narrowing of the tropical precipitation in the Southern Hemisphere may not be realistic.

Like CloudSat rain, the largest CloudSat heavy rain frequencies occur in the ITCZ in both observations and in models. The CESM1 distribution of CloudSat heavy rain is more concentrated than the observed distribution of CloudSat rain. CESM1 underestimates the occurrence frequency of CloudSat heavy rain in the ITCZ by a

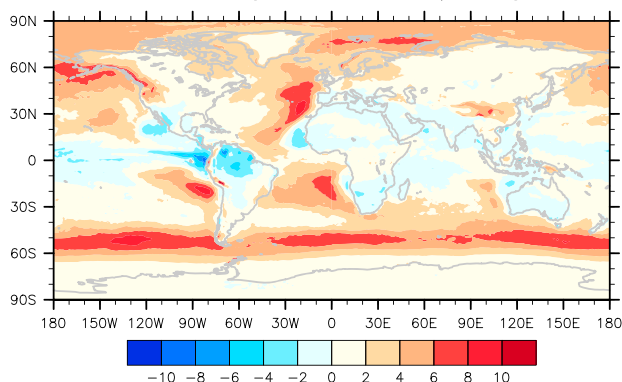
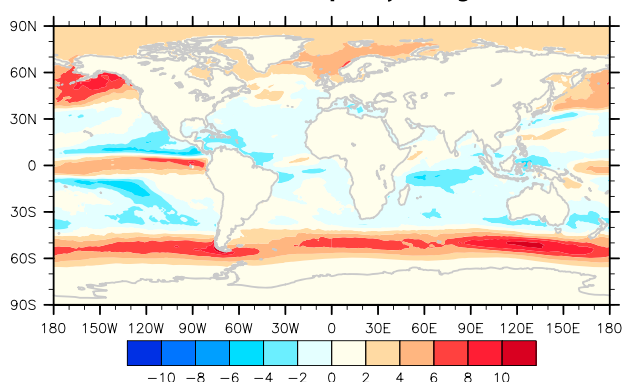
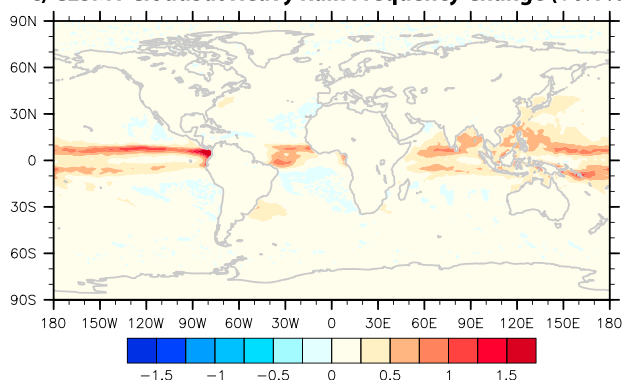
a) CESM1 CloudSat Light Rain Frequency Change (+1.6%)**b) CESM1 CloudSat Rain Frequency Change (+0.6%)****c) CESM1 CloudSat Heavy Rain Frequency Change (+0.1%)**

Figure 10. Global map of CESM1 near-surface rain frequency change (2080 s – 2010 s): (a) CloudSat light rain, (b) CESM1 CloudSat rain, (c) CESM1 heavy rain. Global mean values are reported in parenthesis.

GPCP nor TRMM detect light rain (<1 mm/day; Behrangi et al., 2014; Berg et al., 2010), their light rain comparisons were not robust. Here, for the first time, a quantitative ability to evaluate light rain in climate models is provided. Why is the light rain frequency bias important for climate? Light rain contributes little atmospheric latent heating, so it is not strongly constrained energetically (Pendergrass & Hartmann, 2014). While light rain has little impact on latent heating, light rain still has important impacts on cloud evolution (e.g., see review by Wood, 2012). For example, drizzle influences both cloud lifetime and aerosol scavenging. Excessive drizzle keeps the shallow convective regions pristine, reduces cloud lifetime, and makes low clouds more susceptible to aerosol indirect effects (e.g., Twohy et al., 2005). The mappable diagnostics introduced here provide a simple companion to process-oriented diagnostics developed by Suzuki et al. (2015) and Jing et al. (2017) who also use the CloudSat simulator framework to evaluate model light rain biases.

factor of 2. Over the 21st century, the projected increase in CESM1 CloudSat heavy rain frequency is consistent with increased intensity and the wet-get-wetter hypothesis. Finally, biases in the location of present-day heavy rain are imprinting themselves on future heavy rain changes.

4. Discussion

This study provides new scale-aware and definition-aware diagnostics for evaluation of near-surface precipitation frequency. The new diagnostics fill a need for precipitation frequency diagnostics at a range of intensities that are mappable and robust. With the new diagnostics, a quantitative evaluation of model rain and snow frequency in a range of reflectivity-based intensity classes is now possible. As evidenced by the evaluation of CESM1 in this study, these new diagnostics can quantitatively expose model precipitation frequency biases from light to heavy precipitation. As the new diagnostics are applied to a software package widely adopted by the climate modeling community (COSP), the new diagnostics can be broadly incorporated into model development and evaluation efforts. While the methods here leverage a single spaceborne radar (the 94-GHz CloudSat CPR), the methods are extendable to other current and future spaceborne cloud and precipitation radar missions [e.g., TRMM, Global Precipitation Mission (GPM; Hou et al., 2014), and the 94-GHz EarthCARE (Illingworth et al., 2015)].

Our results reinforce previous studies that found large precipitation frequency model biases but did not use “definition-aware” methods. Comfortingly, our main result—CESM1 rains and snows too often but with insufficient intensity when compared to observations—qualitatively agrees with previous work that was not “definition aware.” For example, Pendergrass and Deser (2017) found that CESM1 had excessive precipitation frequency and insufficient precipitation intensity. McIlholland et al. (2017) find excessive snow frequency in CESM1 when compared to CloudSat observations. Beyond CESM1, Stephens et al. (2010) evaluated several climate and weather models using CloudSat observations in a scale-aware but not definition-aware framework. Their conclusion is that models overestimate rain frequency but underestimate rain intensity. In sum, the “dreary state” of climate models identified by Stephens et al. (2010) is confirmed by this work and quantitatively established in a scale-aware and definition-aware framework.

An easily mappable CloudSat light rain diagnostic is the most novel advance of this study for model evaluation. The climate community is well aware of the difficulty of evaluating light rain in models. For example, Pendergrass and Deser (2017) show that CESM1 has much more light precipitation than GPCP and TRMM, but they also lament that since neither

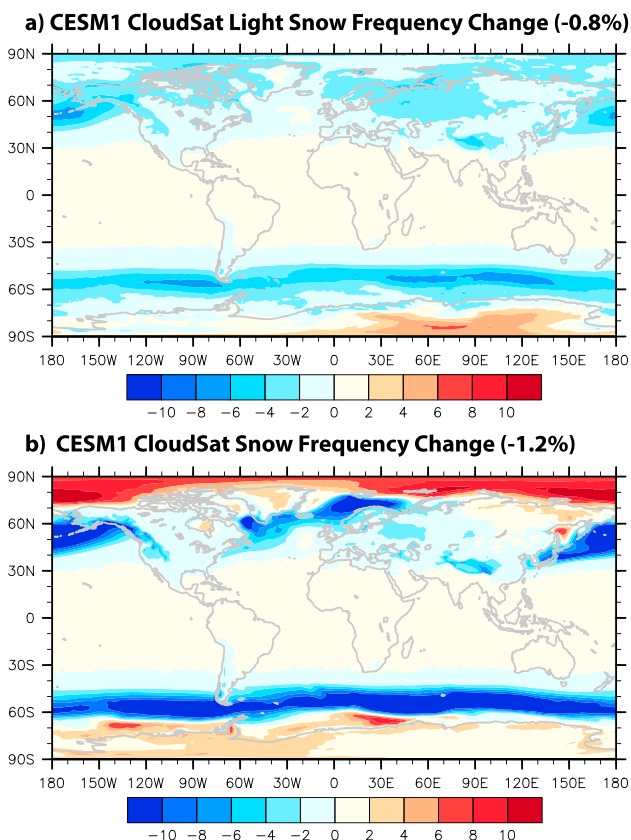


Figure 11. Global map of CESM1 near-surface snow frequency change (2080s – 2010s): (a) CloudSat light snow, (b) CESM1 CloudSat snow. CloudSat light snow and CloudSat snow definitions are based on reflectivity and fraction of ice present (see Table 2). Global mean values are reported in parenthesis.

GPM) would be helpful to add to this forward model-based framework. That said, the spatial distribution of annual mean accumulation closely resembles the spatial distribution of CloudSat rain frequency. When the most common rain intensity contributes most to the total precipitation, the spatial pattern of precipitation frequency will resemble spatial pattern of accumulation (see Figure 7; Pendergrass & Deser, 2017).

Trusting future precipitation changes predicted by models under climate change requires understanding whether or not rain is realistically represented in the present day. Within CESM1, we have evidence for model biases imprinting on future change. For CloudSat heavy rain frequency, future increases map onto present-day biases. In addition, does the excessive precipitation frequency in present-day lead to larger absolute precipitation frequency changes in the future?

Now that diagnostics are available and biases have been robustly exposed—Do we know what causes the biases, and potentially how to fix them. For CESM1, excessive precipitation frequency occurs everywhere, and therefore, the bias is not simply traceable to the representation of just the resolved or just the unresolved precipitation. Tropical biases result from parameterized convective precipitation, while extratropical biases result from resolved large-scale precipitation. Excessive light rain frequency in CESM1 may result in part from the assumption of a Marshall-Palmer exponential drop size distribution for precipitation (Abel & Boutle, 2012). More importantly, CESM1 lacks a subgrid-scale representation of precipitation fraction. Indeed, CESM1 assumes that all clouds precipitate, similar to previous versions of the atmospheric component of CESM1 (Zhang et al., 2010). Interestingly, assuming that all clouds that precipitate is a structural shortcoming to the parameterizations could be the root cause of excessive precipitation frequency in CESM1 when compared to observations.

Another new advance enabled by this work is assessment of modeled snow frequency from CloudSat in a definition-aware and scale-aware framework. The results shown here for CESM1 indicate that snow exhibits the same excessive frequency model bias as rain. Importantly, large changes in CESM1 snow frequency occur in response to future 21st century forcing. CESM1 snow frequency at all subpolar latitudes decreases over the 21st century and turns into rain. CESM1 annual mean snow frequency increases at the high latitudes over the 21st century. Over the Arctic Ocean, increased snow frequency likely results from the additional oceanic moisture source arising from the loss of sea ice (e.g., Bintanja & Selten, 2014). In contrast, increased snowfall over the Greenland and Antarctic ice sheets has been more simply attributed to a warmer atmosphere having more moisture than a colder atmosphere (e.g., Frieler et al., 2015). While the snow change signatures seen in this study are broadly consistent with previous work, a seasonal and surface-type perspective is needed to fully understand the underlying mechanisms and implications for surface albedo and ice sheet mass balance. Indeed, an in-depth analysis of high-latitude snow frequency offers low-hanging fruit for future work using the radar reflectivity-based diagnostics introduced in this study.

Even though the CloudSat radar signal is completely attenuated in heavy rain, the CloudSat heavy rain frequency diagnostics applied here over the ocean are useful and robust. Our comparisons show that CESM1 heavy rain frequency occurs too infrequently and thus has the opposite bias of rain at moderate and light intensities. Since global rainfall must balance atmospheric radiative cooling, excessive frequency of moderate and light rain and insufficient frequency of heavy rain makes physical sense for CESM1. The results here confirm concerns that CESM1 may underestimate precipitation intensity extremes, because it precipitates too frequently. Given their ability to detect heavy rain frequency, the context of spaceborne precipitation radars (e.g., TRMM,

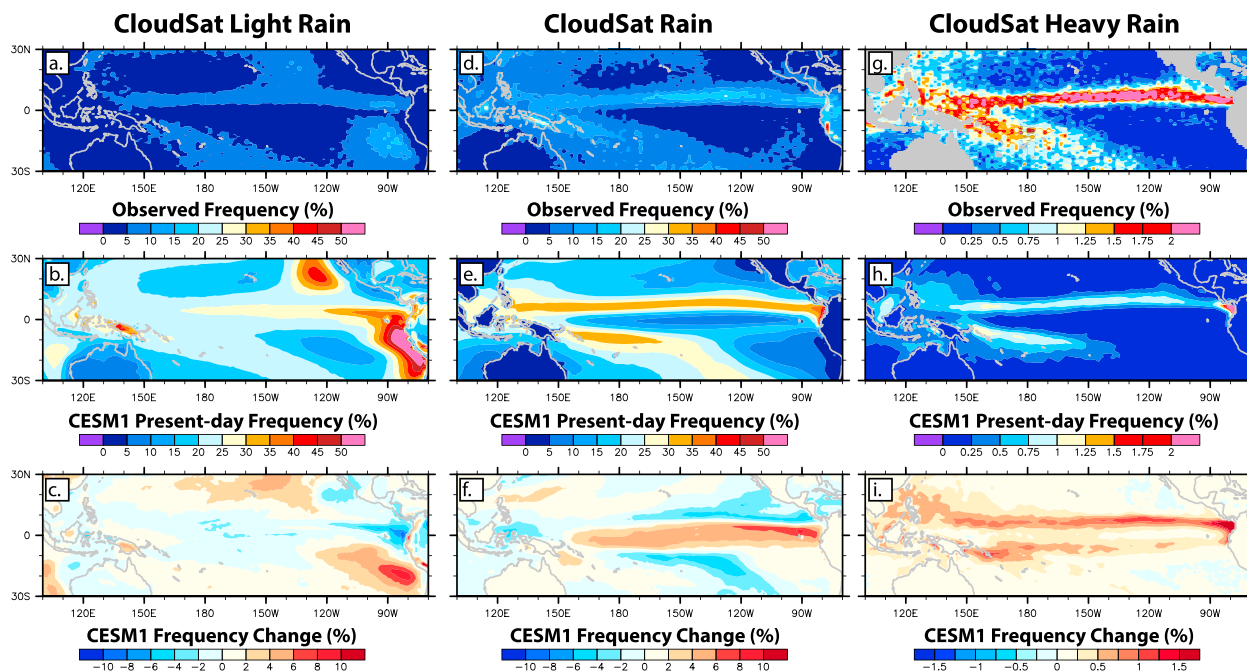


Figure 12. Tropical Pacific regional maps: (a) observed CloudSat light rain, (b) CESM1 present-day CloudSat light rain, (c) CESM1 21st century change (2080 s – 2010 s) in CloudSat light rain, (d–f) as in (a–c) but for CloudSat rain, (g–i) as in (a–c) but for CloudSat heavy rain. See Table 2 for definitions of CloudSat light rain, CloudSat rain, and CloudSat heavy rain.

5. Summary

This study provides new tools that advance our ability to evaluate the spatial distribution of near-surface precipitation frequency in climate models. The introduced diagnostics are scale aware and definition aware and provide assessment capacity for both modeled rain and snow at a range of intensities. Applying these diagnostics to a community climate model used globally for climate research and projections (CESM1), the main findings are excessive precipitation frequency model biases for both rain and snow. The only rain class examined with insufficient frequency was the heaviest rain intensity, which occurs rarely. Implications for the water and energy cycle of CESM1 are numerous. For example, the results establish that CESM1 precipitates too frequently with insufficient intensity. Many fully explored this study whose primary aim is to introduce the diagnostics and show global results. Future work should continue to develop metrics for climate model evaluation that are both scale aware and definition aware. More could be done to leverage not only CloudSat observations but also observations from precipitation radars such as TRMM and GPM in frameworks that are definition aware and scale aware and enable robust constraints and understanding of modeled energy and water cycles. Specifically, combining TRMM/GPM/CloudSat observations would enable the most complete evaluation of the entire distribution of precipitation rates (i.e., from light to heavy precipitation rates).

Acknowledgments

We thank Brian Eaton and Dave Bailey for their help in troubleshooting CESM simulations and code. We thank Matt Lebsack and two anonymous reviewers for their helpful suggestions. We acknowledge high-performance computing support provided by NCAR's Computational and Information Systems Laboratory, sponsored by the National Science Foundation. All model simulations are archived on the National Center for Atmospheric Research (NCAR) High Performance Storage System (HPSS) Repository at /home/jenkay/csm. The source code for the model used in this study, the Community Earth System Model (CESM) version 5, is freely available at <http://www2.cesm.ucar.edu/>. J. E. K., T. S. L., and V. Y. were supported by NASA grant 15-CCST15-0025. R. G. was supported by Centre National d'Etudes Spatiales (CNES).

References

Abel, S. J., & Boutle, I. A. (2012). An improved representation of the raindrop size distribution for single-moment microphysics schemes. *Quarterly Journal of the Royal Meteorological Society*, 138(669), 2151–2162. <https://doi.org/10.1002/qj.1949>

Adler, R. F., Huffman, G. J., Chang, A., Ferraro, R., Xie, P. P., Janowiak, J., et al. (2003). The version-2 Global Precipitation Climatology Project (GPCP) monthly precipitation analysis (1979–present). *Journal of Hydrometeorology*, 4(6), 1147–1167. [https://doi.org/10.1175/1525-7541\(2003\)004%3C1147:TVGPCP%3E2.0.CO;2](https://doi.org/10.1175/1525-7541(2003)004%3C1147:TVGPCP%3E2.0.CO;2)

Barnett, T. P., Adam, J. C., & Lettenmaier, D. P. (2005). Potential impacts of a warming climate on water availability in snow-dominated regions. *Nature*, 438(7066), 303–309. <https://doi.org/10.1038/nature04141>

Battaglia, A., Haynes, J. M., L'Ecuyer, T., & Simmer, C. (2008). Identifying multiple-scattering- affected profiles in CloudSat observations over the oceans. *Journal of Geophysical Research*, 113, D00A17. <https://doi.org/10.1029/2008JD009960>

Behrangi, A., Lebsack, M., Wong, S., & Lambrightsen, B. (2012). On the quantification of oceanic rainfall using spaceborne sensors. *Journal of Geophysical Research*, 117, D20105. <https://doi.org/10.1029/2012JD017979>

Behrangi, A., Stephens, G., Adler, R. F., Huffman, G. J., Lambrightsen, B., & Lebsack, M. (2014). An update on the oceanic precipitation rate and its zonal distribution in light of advanced observations from space. *Journal of Climate*, 27, 3957–3965. <https://doi.org/10.1175/JCLI-D-13-00679.1>

Berg, W., L'Ecuyer, T., & Haynes, J. M. (2010). The distribution of rainfall over oceans from spaceborne radars. *Journal of Applied Meteorology and Climatology*, 49(3), 535–543. <https://doi.org/10.1175/2009JAMC2330.1>

Bintanja, R., & Selten, F. M. (2014). Future increases in Arctic precipitation linked to local evaporation and sea-ice retreat. *Nature*, 509(7501), 479–482. <https://doi.org/10.1038/nature13259>

Bodas-Salcedo, A., Webb, M. J., Bony, S., Chepfer, H., Dufresne, J. L., Klein, S. A., et al. (2011). COSP: Satellite simulation software for model assessment. *Bulletin of the American Meteorological Society*, 92(8), 1023–1043. <https://doi.org/10.1175/2011BAMS2856.1>

Bodas-Salcedo, A., Webb, M. J., Brooks, M. E., Ringer, M. A., William, K. D., Milton, S. F., & Wilson, D. R. (2008). Evaluating cloud systems in the Met Office global forecast model using simulated CloudSat radar reflectivities. *Journal of Geophysical Research*, 113, D00A13. <https://doi.org/10.1029/2007JD009620>

Bony, S., Bellon, G., Klocke, D., Sherwood, S., Fergepin, S., & Denvil, S. (2013). Robust direct effect of carbon dioxide on tropical circulation and regional precipitation. *Nature Geoscience*, 6(6), 447–451. <https://doi.org/10.1038/ngeo1799>

Boucher, O., Randall, D., Artaxo, P., Bretherton, C., Feingold, G., Forster, P., et al. (2013). Clouds and Aerosols. In T. F. Stocker, et al. (Eds.), *Climate change 2013: The physical science basis. Contribution of Working Group I to the Fifth Assessment Report of the Intergovernmental Panel on Climate Change* (pp. 571–657). Cambridge, UK and New York: Cambridge University Press.

Byrne, M. P., & Schneider, T. (2016). Narrowing of the ITCZ in a warming climate: Physical mechanisms. *Geophysical Research Letters*, 43, 11,350–11,357. <https://doi.org/10.1002/2016GL070396>

Chou, C., & Neelin, J. D. (2004). Mechanisms of global warming impacts on regional tropical precipitation. *Journal of Climate*, 17(13), 2688–2701. [https://doi.org/10.1175/1520-0442\(2004\)017%3C2688:MOGWIO%3E2.0.CO;2](https://doi.org/10.1175/1520-0442(2004)017%3C2688:MOGWIO%3E2.0.CO;2)

Dai, A. (2006). Precipitation characteristics in eighteen coupled climate models. *Journal of Climate*, 19, 4605–4630. <https://doi.org/10.1175/JCLI3884.1>

Déry, S. J., & Brown, R. D. (2007). Recent Northern Hemisphere snow cover extent trends and implications for the snow-albedo feedback. *Geophysical Research Letters*, 34, L22504. <https://doi.org/10.1029/2007GL031474>

Di Michele, S., Ahlgren, M., Forbes, R., Kulie, M., Bennartz, R., Janíková, M., & Bauer, P. (2012). Interpreting an evaluation of the ECMWF global model with CloudSat observations: Ambiguities due to radar reflectivity forward operator uncertainties. *Quarterly Journal of the Royal Meteorological Society*, 138(669), 2047–2065. <https://doi.org/10.1002/qj.1936>

Ellis, T. D., L'Ecuyer, T., Haynes, J. M., & Stephens, G. L. (2009). How often does it rain over the global oceans? The perspective from CloudSat. *Geophysical Research Letters*, 36, L03815. <https://doi.org/10.1029/2008GL036728>

English, J. M., Kay, J. E., Gettelman, A., Liu, X., Wang, Y., Zhang, Y., & Chepfer, H. (2014). Contributions of clouds, surface albedos, and mixed-phase ice nucleation schemes to Arctic radiation biases in CAM5. *Journal of Climate*, 27(13), 5174–5197. <https://doi.org/10.1175/JCLI-D-13-00608.1>

Fabry, F., & Zawadzki, I. (1995). Long-term radar observations of the melting layer precipitation and their interpretation. *Journal of the Atmospheric Sciences*, 52(7), 838–851. [https://doi.org/10.1175/1520-0469\(1995\)052%3C838:LTROOT%3E2.0.CO;2](https://doi.org/10.1175/1520-0469(1995)052%3C838:LTROOT%3E2.0.CO;2)

Flanner, M. G., Shell, K. M., Barlage, M., Perovich, D. K., & Tschudi, M. A. (2011). Radiative forcing and albedo feedback from the Northern Hemisphere cryosphere between 1979 and 2008. *Nature Geoscience*, 4(3), 151–155. <https://doi.org/10.1038/ngeo1062>

Flato, G., Marotzke, J., Abiodun, B., Braconnot, P., Chou, S. C., Collins, W., et al. (2013). Evaluation of climate models. In T. F. Stocker, et al. (Eds.), *Climate change 2013: The physical science basis. Contribution of Working Group I to the Fifth Assessment Report of the Intergovernmental Panel on Climate Change* (pp. 741–866). Cambridge, UK and New York: Cambridge University Press.

Frieler, K., Clark, P. U., He, F., Buijzer, C., Reese, R., Ligtenberg, S. R. M., et al. (2015). Consistent evidence of increasing Antarctic accumulation with warming. *Nature Climate Change*, 5(4), 348–352. <https://doi.org/10.1038/nclimate2574>

Greve, P., Orlowsky, B., Mueller, B., Sheffield, J., Reichstein, M., & Seneviratne, S. I. (2014). Global assessment of trends in wetting and drying over land. *Nature Geoscience*, 7(10), 716–721. <https://doi.org/10.1038/ngeo2247>

Haynes, J., Marchand, R., Luo, Z., Bodas-Salcedo, A., & Stephens, G. (2007). A multipurpose radar simulation package: Quickbeam. *Bulletin of the American Meteorological Society*, 88(11), 1723–1728. <https://doi.org/10.1175/BAMS-88-11-1723>

Haynes, J. M., L'Ecuyer, T. S., Stephens, G. L., Miller, S. D., Mitrescu, C., Wood, N. B., & Tanelli, S. (2009). Rainfall retrieval over the ocean with spaceborne W-band radar. *Journal of Geophysical Research*, 114, D00A22. <https://doi.org/10.1029/2008JD009973>

Held, I. M., & Soden, B. J. (2006). Robust responses of the hydrological cycle to global warming. *Journal of Climate*, 19(21), 5686–5699. <https://doi.org/10.1175/JCLI3990.1>

Hogan, R. J., & Battaglia, A. (2008). Fast lidar and radar multiple-scattering models. Part II: Wide-angle scattering using the time-dependent two-stream approximation. *Journal of the Atmospheric Sciences*, 65(12), 3636–3651. <https://doi.org/10.1175/2008JAS2643.1>

Hong, Y., Adler, R. F., Hossain, F., Curtis, S., & Huffman, G. J. (2007). A first approach to global runoff simulation using satellite rainfall estimation. *Water Resources Research*, 43, W08502. <https://doi.org/10.1029/2006WR005739>

Hou, A. Y., Kakar, R. K., Neeck, S., Azarbarzin, A. A., Kummerow, C. D., Kojima, M., et al. (2014). The global precipitation measurement mission. *Bulletin of the American Meteorological Society*, 95, 701–722. <https://doi.org/10.1175/BAMS-D-13-00164.1>

Hurrell, J. W., Holland, M. M., Gent, P. R., Ghan, S., Kay, J. E., Kushner, P. J., et al. (2013). The community Earth system model: A framework for collaborative research. *Bulletin of the American Meteorological Society*, 94(9), 1339–1360. <https://doi.org/10.1175/BAMS-D-12-00121.1>

Illingworth, A. J., Barker, H. W., Beljaars, A., Ceccaldi, M., Chepfer, H., Clerbaux, N., et al. (2015). The EarthCARE satellite: The next step forward in global measurements of clouds, aerosols, precipitation, and radiation. *Bulletin of the American Meteorological Society*, 96, 1311–1332. <https://doi.org/10.1175/BAMS-D-12-00227.1>

Jing, X., Suzuki, K., Guo, H., Goto, D., Ogura, T., Koshiro, T., & Mülmenstädt, J. (2017). A multimodel study on warm precipitation biases in global models compared to satellite observations. *Journal of Geophysical Research: Atmospheres*, 122, 11,806–11,824. <https://doi.org/10.1002/2017JD027310>

Kay, J. E., Bourdages, L., Chepfer, H., Miller, N., Morrison, A., Yettella, V., & Eaton, B. (2016). Evaluating and improving cloud phase in the community atmosphere model version 5 using spaceborne lidar observations. *Journal of Geophysical Research: Atmospheres*, 121, 4162–4176. <https://doi.org/10.1002/2015JD024699>

Kay, J. E., Deser, C., Phillips, A., Mai, A., Hannay, C., Strand, G., et al. (2015). The Community Earth System Model (CESM) large ensemble project: A community resource for studying climate change in the presence of internal climate variability. *Bulletin of the American Meteorological Society*, 96(8), 1333–1349. <https://doi.org/10.1175/BAMS-D-13-00255.1>

Kay, J. E., Hillman, B., Klein, S., Zhang, Y., Medeiros, B., Gettelman, G., et al. (2012). Exposing global cloud biases in the Community Atmosphere Model (CAM) using satellite observations and their corresponding instrument simulators. *Journal of Climate*, 25(15), 5190–5207. <https://doi.org/10.1175/JCLI-D-11-00469.1>

Kim, D. K., Sperber, K., Stern, W., Waliser, D., Kang, I.-S., Maloney, E., et al. (2009). Application of MJO simulation diagnostics to climate models. *Journal of Climate*, 22(23), 6413–6436. <https://doi.org/10.1175/2009JCLI3063.1>

Klein, S. A., & Jakob, C. (1999). Validation and sensitivities of frontal clouds simulated by the ECMWF model. *Monthly Weather Review*, 127(10), 2514–2531. [https://doi.org/10.1175/1520-0493\(1999\)127%3C2514:VASOFC%3E2.0.CO;2](https://doi.org/10.1175/1520-0493(1999)127%3C2514:VASOFC%3E2.0.CO;2)

Knutti, R., Masson, D., & Gettelman, A. (2013). Climate model genealogy: Generation CMIP5 and how we got there. *Geophysical Research Letters*, 40, 1194–1199. <https://doi.org/10.1002/grl.50256>

Kummerow, C., Simpson, J., Thiele, O., Barnes, W., Chang, A. T. C., Stocker, E., et al. (2000). The status of the tropical rainfall measuring mission (TRMM) after two years in orbit. *Journal of Applied Meteorology*, 39, 1965–1982. [https://doi.org/10.1175/1520-0450\(2001\)040%3C1965:TSOTTR%3E2.0.CO;2](https://doi.org/10.1175/1520-0450(2001)040%3C1965:TSOTTR%3E2.0.CO;2)

L'Ecuyer, T. S., & Stephens, G. L. (2007). The tropical atmospheric energy budget from the TRMM perspective. Part II: Evaluating GCM representations of the sensitivity of regional energy and water cycles to the 1998–99 ENSO cycle. *Journal of Climate*, 20(18), 4548–4571. <https://doi.org/10.1175/JCLI4207.1>

Lu, J., Vecchi, G. A., & Reichler, T. (2007). Expansion of the Hadley cell under global warming. *Geophysical Research Letters*, 34, L06805.

Marchand, R. T., Haynes, J., Mace, G. G., Ackerman, T., & Stephens, G. (2009). A comparison of simulated cloud radar output from the multiscale modeling framework global climate model with CloudSat cloud radar observations. *Journal of Geophysical Research*, 114, D00A20. <https://doi.org/10.1029/2008JD009790>

McIlholland, E. A., L'Ecuyer, T. S., & Miller, N. B. (2017). Observational evidence linking Arctic supercooled liquid cloud biases in CESM to snowfall processes. *Journal of Climate*, 30(12), 4477–4495. <https://doi.org/10.1175/JCLI-D-16-0666.1>

Morrison, H., & Gettelman, A. (2008). A new two-moment bulk stratiform cloud microphysics scheme in the NCAR Community Atmosphere Model (CAM3). Part I: Description and numerical tests. *Journal of Climate*, 21(15), 3642–3659. <https://doi.org/10.1175/2008JCLI2105.1>

Nam, C. C. W., Quaas, J., Neggers, R., Siegenthaler-Le Drian, C., & Isotta, F. (2014). Evaluation of boundary layer cloud parameterizations in the ECHAM5 general circulation model using CALIPSO and CloudSat satellite data. *Journal of Advances in Modeling Earth Systems*, 6(2), 300–314. <https://doi.org/10.1002/2013MS000277>

Nesbitt, S. W., & Zipser, E. J. (2003). The diurnal cycle of rainfall and convective intensity according to three years of TRMM measurements. *Journal of Climate*, 16(10), 1456–1475. <https://doi.org/10.1175/1520-0442-16.10.1456>

Palerme, C., Kay, J. E., Gentron, C., L'Ecuyer, T., Wood, N. B., & Claud, C. (2014). How much snow falls on the Antarctic ice sheet? *The Cryosphere*, 8(4), 1577–1587. <https://doi.org/10.5194/tc-8-1577-2014>

Park, S., Bretherton, C. S., & Rasch, P. J. (2014). Integrating cloud processes in the Community Atmosphere Model, version 5. *Journal of Climate*, 27(18), 6821–6856. <https://doi.org/10.1175/JCLI-D-14-00087.1>

Pendergrass, A. G., & Deser, C. (2017). Characterizing the climatological distribution of rain frequency and intensity. *Journal of Climate*, 30(15), 5985–6003. <https://doi.org/10.1175/JCLI-%20D-16-0684.1>

Pendergrass, A. G., & Hartmann, D. L. (2014). The atmospheric energy constraint on global-mean precipitation change. *Journal of Climate*, 27(2), 757–768. <https://doi.org/10.1175/JCLI-D-13-%2000163.1>

Rignot, E., Velicogna, I., van den Broeke, M. R., Monaghan, A., & Lenaerts, J. T. M. (2011). Acceleration of the contribution of the Greenland and Antarctic ice sheets to sea level rise. *Geophysical Research Letters*, 38, L05503. <https://doi.org/10.1029/2011GL046583>

Smalley, M., L'Ecuyer, T., Lebsack, M., & Haynes, J. (2014). A comparison of precipitation occurrence from the NCEP stage IV QPE product and the CloudSat profiling radar. *Journal of Hydrometeorology*, 15(1), 444–458. <https://doi.org/10.1175/JHM-D-13-048.1>

Stephens, G. L., & Ellis, T. D. (2008). Controls of global-mean precipitation increases in global warming GCM experiments. *Journal of Climate*, 21(23), 6141–6155. <https://doi.org/10.1175/2008JCLI2144.1>

Stephens, G. L., L'Ecuyer, T., Forbes, R., Gettelman, A., Golaz, J. C., Bodas-Salcedo, A., et al. (2010). Dreary state of precipitation in global models. *Journal of Geophysical Research*, 115, D24211. <https://doi.org/10.1029/2010JD014532>

Stephens, G. L., Vane, D. G., Tanelli, S., Im, E., Durden, S., Rokey, M., et al. (2008). CloudSat mission: Performance and early science after the first year of operation. *Journal of Geophysical Research*, 113, D00A18. <https://doi.org/10.1029/2008JD009982>

Suzuki, K., Stephens, G. L., Bodas-Salcedo, A., Wang, M., Golaz, J.-C., Yokohata, T., & Tsuyoshi, K. (2015). Evaluation of the warm rain formation process in global models with satellite observations. *Journal of the Atmospheric Sciences*, 72(10), 3996–4014. <https://doi.org/10.1175/JAS-D-14-0265.1>

Swales, D. J., Pincus, R., & Bodas-Salcedo, A. (2018). The cloud feedback model intercomparison project observational simulator package: Version 2. *Geoscientific Model Development*, 11, 77–81. <https://doi.org/10.5194/gmd-11-77-2018>

Teixeira, J., Waliser, D., Ferraro, R., Gleckler, P., Lee, T., & Potter, G. (2014). Satellite observations for CMIP5: The genesis of Obs4MIPs. *Bulletin of the American Meteorological Society*, 95(9), 1329–1334. <https://doi.org/10.1175/BAMS-D-12-00240.1>

Twohy, C. H., Petters, M. D., Snider, J. R., Stevens, B., Tahnk, W., Wetzel, M., et al. (2005). Evaluation of the aerosol indirect effect in marine stratocumulus clouds: Droplet number, size, liquid water path, and radiative impact. *Journal of Geophysical Research*, 110, D08203. <https://doi.org/10.1029/2004JD005116>

Vecchi, G. A., & Soden, B. J. (2007). Global warming and the weakening of the tropical circulation. *Journal of Climate*, 20(17), 4316–4340. <https://doi.org/10.1175/JCLI4258.1>

Wang, Y., Ma, P.-L., Jiang, J., Su, H., & Rasch, P. (2016). Towards reconciling the influence of atmospheric aerosols and greenhouse gases on light precipitation changes in eastern China. *Journal of Geophysical Research: Atmospheres*, 121, 5878–5887. <https://doi.org/10.1002/2016JD024845>

Webb, M. J., Andrews, T., Bodas-Salcedo, A., Bony, S., Bretherton, C. S., Chadwick, R., et al. (2017). The Cloud Feedback Model Intercomparison Project (CFMIP) contribution to CMIP6. *Geoscientific Model Development*, 10(1), 359–384. <https://doi.org/10.5194/gmd-10-359-%202017>

Wood, R. (2012). REVIEW stratocumulus clouds. *Monthly Weather Review*, 140(8), 2373–2423. <https://doi.org/10.1175/MWR-D-11-00121.1>

Yettella, V., & Kay, J. E. (2017). How will precipitation change in extratropical cyclones as the planet warms?: Insights from a large initial condition climate model ensemble. *Climate Dynamics*, 49(5–6), 1765–1781. <https://doi.org/10.1007/s00382-016-3410-2>

Yuter, S. E., & Houze, R. A. (1995). Three-dimensional kinematic and microphysical evolution of Florida cumulonimbus. Part II: Frequency distributions of vertical velocity, reflectivity, and differential reflectivity. *Monthly Weather Review*, 123(7), 1941–1963. [https://doi.org/10.1175/1520-0493\(1995\)123%3C1941:TDKAME%3E2.0.CO;2](https://doi.org/10.1175/1520-0493(1995)123%3C1941:TDKAME%3E2.0.CO;2)

Zhang, Y., Klein, S. A., Boyle, J., & Mace, G. G. (2010). Evaluation of tropical cloud and precipitation statistics of Community Atmosphere Model version 3 using CloudSat and CALIPSO data. *Journal of Geophysical Research*, 115, D12205. <https://doi.org/10.1029/2009JD012006>

Zhang, Y., Klein, S. A., Liu, C., Tian, B., Marchand, R. T., Haynes, J. M., et al. (2008). On the diurnal cycle of deep convection, high-level cloud, and upper troposphere water vapor in the multiscale modeling framework. *Journal of Geophysical Research*, 113, D16105. <https://doi.org/10.1029/2008JD009905>

Zipser, E. J., Liu, C., Cecil, D. J., Nesbitt, S. W., & Yorty, D. P. (2006). Where are the most intense thunderstorms on earth? *Bulletin of the American Meteorological Society*, 87(8), 1057–1071. <https://doi.org/10.1175/BAMS-87-8-1057>